Solving Multiperiod OPF Problems using an AC-QP Algorithm Initialized with an SOCP Relaxation

Jennifer F. Marley, Daniel K. Molzahn, and Ian A. Hiskens

***Abstract*—Renewable generation and energy storage are playing an ever increasing role in power systems. Hence, there is a growing need for integrating these resources into the optimal power flow (OPF) problem. While storage devices are important for mitigating renewable variability, they introduce temporal coupling in the OPF constraints, resulting in a multiperiod OPF formulation. This paper explores a solution method for multiperiod AC OPF that combines a successive quadratic programming approach (AC-QP) with a second-order cone programming (SOCP) relaxation of the OPF problem. The SOCP relaxation's solution is used to initialize the AC-QP OPF algorithm. Additionally, the lower bound on the objective value obtained from the SOCP relaxation provides a measure of solution quality. This combined method is demonstrated on several test cases with up to 4259 nodes and a time horizon of 8 time steps. A comparison of initialization schemes indicates that the SOCP-based approach offers improved convergence rate, execution time and solution quality.**

***Index Terms*—Optimal power flow, convex relaxation, global solution, large-scale power system optimization.**

I. Introduction

The goal of an optimal power flow (OPF) is to determine the optimal operating point for an electric power system relative to a specified objective, such as minimizing generation cost, losses, or renewable spillage. In optimizing the specified objective, the solution must satisfy engineering and physical constraints. These consist of the nonlinear AC power flow equations, line-flow limits, and operational limits on control variables (including voltage magnitude limits and generator active and reactive power output limits) [1].

Many solution methods have been applied to AC OPF problems. These include gradient methods, Newton's method, successive quadratic programming methods (AC-QP), and interior point methods [1]–[4]. Additionally, the DC OPF formulation is often used to approximate the AC OPF problem as a quadratic program [5]–[7]. Due to its convexity and scalability to large networks, the DC OPF approximation offers a variety of computational benefits. Under normal operating conditions, it usually provides a reasonable approximation of the AC OPF problem [8]. However, it does not necessarily result in an AC feasible solution, and there are cases where the DC power flow has non-negligible errors compared to the AC power flow [9], [10].

The AC-QP OPF algorithm is the focus of this paper. This algorithm uses a successive linearization procedure implemented with a quadratic program (QP) [1]. The AC-QP algorithm has the advantage of providing an AC-feasible solution, as each iteration solves an AC power flow. Additionally, solvers for quadratic programs and AC power flow methods scale well, making the AC-QP algorithm applicable to large systems. However, these advantages come with some trade-offs: this method is dependent on a converged AC power flow and the optimal solution is sensitive to the initialization. Depending on the proximity of the initialization to the globally optimal solution, the AC-QP algorithm runs the risk of failing to converge or converging to a local solution. Thus, developing better initialization procedures is important for improving the performance of the AC-QP algorithm. The initialization challenges of the AC-QP algorithm are particularly pronounced following a large change in loading and/or network topology which results in a significant change in the operating point (e.g., contingency events) as well as for planning scenarios which offer limited prior knowledge of the solution.

There have been many recent developments in applying semidefinite programming (SDP) and second-order cone programming (SOCP) methods to formulate convex relaxations of the OPF problem. Several examples of these relaxations can be found in [11]–[23]. Convex relaxations lower bound the objective value, can certify problem infeasibility, and, in many cases, provide the global solution (i.e., the relaxations are often *exact*). However, there are many practical problems for which existing relaxations fail to be exact, so the solutions they produce are not physically realizable [24]–[26]. While solvers for the SDP relaxations are available for moderately sized networks, application to large networks is generally more complicated than other solution methods [14], [18]. Thus, further research is needed to employ these methods in real-time applications for large networks. In contrast, the SOCP relaxation in [13] can be quickly solved for large networks to obtain a lower bound on the globally optimal objective value and an initialization for the AC-QP algorithm. Providing a procedure for combining these two methods in this manner is the focus of this paper.

Renewable generation offers economic and environmental benefits, but also challenges system reliability due to its inherent variability. Storage devices provide a means of (at least partially) mitigating this variability. Thus, OPF methods must be adapted to incorporate both renewable generation and storage [27]. However, the state-of-charge dynamics of storage devices [28] introduce temporal coupling, requiring a multiperiod OPF formulation.

Several multiperiod OPF formulations that integrate renewable generation and storage use a horizon of 24 hours. However, computation time may be excessive when consid-

Research supported by the Department of Energy, ARPA-E Award No. DE-AR0000232, Green Electricity Network Integration (GENI) Program, and by the National Science Foundation through award CNS-1238962.

ering such a long horizon, even for mid-sized systems. As a result, formulations often rely upon the DC power flow approximation, as in [29], or are applicable only to relatively small networks, as in [30]. The algorithm developed in this paper is motivated by on-line applications and so considers an 8-step time horizon in order to meet solution-time constraints. The examples provided in Section III suggest, however, that longer horizons are quite feasible. A 30-minute step is used in the examples, giving a 4-hour horizon, though the choice of time-step has negligible impact on the proposed algorithm.

Other work in multiperiod AC OPF with storage models includes the formulations in [31] and [32]. These approaches establish an SDP relaxation of a multiperiod OPF problem with storage, but do not consider the SOCP relaxation, and do not provide a mechanism for addressing cases where the relaxation is not exact. Furthermore, [31] does not consider storage devices that have non-ideal charge/discharge efficiencies, while [32] considers non-ideal efficiencies but allows non-physical simultaneous charging and discharging.

This paper presents multiperiod versions of both an AC-QP algorithm and an SOCP relaxation which include renewable generation and storage devices that have non-ideal charging and discharging efficiencies. Using the SOCP relaxation's solution to initialize the AC-QP algorithm enables consideration of problems for which the SOCP relaxation is not exact.

The paper is organized as follows. Section II describes two formulations of the OPF problem with storage and wind: an SOCP relaxation and an AC-QP algorithm. Section III presents results for several test cases in order to demonstrate the benefits of the SOCP initialization compared to two other methods. Section IV concludes the paper.

II. Problem Formulation and Solution Algorithm

This section presents a multiperiod OPF formulation with energy storage devices, including non-ideal charge and discharge efficiencies. A convex SOCP relaxation of this problem is then presented, followed by the AC-QP algorithm. Solution of the SOCP relaxation provides both an initialization for the AC-QP algorithm and a lower bound on the objective value, with the latter forming a convenient measure of solution quality.

A. Multiperiod OPF Problem Formulation

The OPF problem seeks to minimize generation cost while satisfying power balance constraints and operational limits on control variables. The formulation used in this paper includes both storage devices and wind generation.

Consider an n-bus power system with buses in the set $\mathcal{N} = \{1, \ldots, n\}$. Define the set of buses with traditional generators as $\mathcal{G}$, each with an associated convex quadratic cost curve $C_i(P_{g,i}) = c_{2,i}P_{g,i}^2 + c_{1,i}P_{g,i} + c_{0,i}$. Let $\mathcal{S}$ denote the set of storage buses and $\mathcal{W}$ denote the set of buses with wind generation. The slack bus is denoted by $slack$.

We use the line model shown in Fig. 1 with an ideal transformer that has a specified turns ratio $\tau_{ij}e^{\mathbf{j}\theta_{shift,ij}}: 1$ in series with a Π-circuit with series impedance $R_{ij} + \mathbf{j}X_{ij}$ and shunt admittance $\mathbf{j}b_{sh,ij}$, where $\mathbf{j}$ is the imaginary unit.

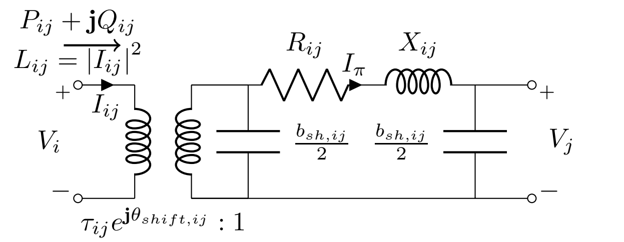

Fig. 1. Line model.

The corresponding series admittance is given by $g_{ij} + jb_{ij} = 1/(R_{ij} + jX_{ij})$. The active and reactive flows into the line's terminal i are denoted P_{ij} and Q_{ij} respectively. The squared current flow is given by L_{ij}, where I_{ij} represents the current flow into terminal i. Similarly, I_π gives the current flow in the π circuit. The voltages across the i and j terminals are represented by V_i and V_j respectively. The set of lines is denoted by $\mathcal{L}$ with $(i, j) \in \mathcal{L}$ indicating that the ideal transformer is at end i of the line. The maximum apparent power flow on line (i, j) is S_{ij}^{max}.

The time horizon is denoted by $\mathcal{T} = \{0, \ldots, T-1\}$, and the time steps are indexed by t. The length of each time step is T_s.

Upper and lower limits on active and reactive power injection at generator bus $i \in \mathcal{G}$ are denoted by $P_{g,i}^{max}$, $P_{g,i}^{min}$ and $Q_{g,i}^{max}$, $Q_{g,i}^{min}$, respectively. This formulation models storage at bus $i \in \mathcal{S}$ as a sink or source of active power with charging and discharging efficiencies $\eta_{c,i}$ and $\eta_{d,i}$, respectively, and corresponding maximum rates $R_{c,i}^{max}$ and $R_{d,i}^{max}$. The initial and final state of charge are e_i^{init} and e_i^{term}, respectively, and the maximum state of charge is E_i. Wind generation at bus $i \in \mathcal{W}$ and time $t \in \mathcal{T}$ is modeled as a source of active power injection with maximum value $W_i^{max}(t)$, zero marginal cost and full curtailment allowed.

The decision variables are the (complex) voltages at each bus and each time, $V_i(t) = |V_i(t)|\angle\theta_i(t)$, $i \in \mathcal{N}$, $t \in \mathcal{T}$, and the battery state of charge $e_i(t)$ for each storage device $i \in \mathcal{S}$ and time $t \in \mathcal{T}$. If positive, the charging rate at time $t \in \mathcal{T}$ is $r_{c,i}(t) = (e_i(t+1) - e_i(t))/(T_s\eta_{c,i})$. Otherwise, the discharge rate at time $t \in \mathcal{T}$ is $r_{d,i}(t) = \eta_{d,i}(e_i(t) - e_i(t+1))/T_s$. As modeled by the power flow equations, the voltages are dependent upon power injections into the network given by $P_{g,i}(t)$, $Q_{g,i}(t)$, $i \in \mathcal{G}$; $P_{w,i}(t)$, $i \in \mathcal{W}$; $r_{d,i}(t) - r_{c,i}(t)$, $i \in \mathcal{S}$; and the active and reactive power loads $P_{d,i}(t)$, $Q_{d,i}(t)$, $i \in \mathcal{N}$ at all times $t \in \mathcal{T}$. The shunt admittance at bus $i \in \mathcal{N}$ is given by $g_{sh,i} + \mathbf{j}b_{sh,i}$. The upper and lower limits on the voltage magnitude at bus $i \in \mathcal{N}$ are V_i^{max} and V_i^{min}, respectively.

With these definitions, the multiperiod OPF problem can be expressed as:

$$\min \sum_{t\in\mathcal{T}}\sum_{i\in\mathcal{G}} C_i(P_{g,i}(t)) \qquad \text{subject to } (\forall t \in \mathcal{T}) \tag{1a}$$

$$P_{g,i}^{min} \le P_{g,i}(t) \le P_{g,i}^{max} \qquad \forall i \in \mathcal{G} \tag{1b}$$

$$Q_{g,i}^{min} \le Q_{g,i}(t) \le Q_{g,i}^{max} \qquad \forall i \in \mathcal{G} \tag{1c}$$

$$0 \le P_{w,i}(t) \le W_i^{max}(t) \qquad \forall i \in \mathcal{W} \tag{1d}$$

$$0 \le r_{c,i}(t) \le R_{c,i}^{max} \qquad \forall i \in \mathcal{S} \tag{1e}$$

$$0 \le r_{d,i}(t) \le R_{d,i}^{max} \qquad \forall i \in \mathcal{S} \tag{1f}$$

$$0 \leq e_i(t) \leq E_i \qquad \forall i \in \mathcal{S} \qquad (1g)$$
$$e_i(0) = e_i^{init} \qquad \forall i \in \mathcal{S} \qquad (1h)$$
$$e_i(T) = e_i^{term} \qquad \forall i \in \mathcal{S} \qquad (1i)$$
$$T_s\left(\eta_{c,i} r_{c,i}(t) - \frac{r_{d,i}(t)}{\eta_{d,i}}\right) = e_i(t+1) - e_i(t) \quad \forall i \in \mathcal{S} \qquad (1j)$$
$$r_{c,i}(t)\, r_{d,i}(t) = 0 \qquad \forall i \in \mathcal{S} \qquad (1k)$$
$$V_i^{min} \leq |V_i(t)| \leq V_i^{max} \qquad \forall i \in \mathcal{N} \qquad (1l)$$
$$\theta_{slack}(t) = 0 \qquad (1m)$$
$$P_{ij}(t) = |V_i(t)|^2 g_{ij}/\tau_{ij}^2 - |V_i(t)||V_j(t)|[g_{ij}\cos(\theta_{ij}(t)) + b_{ij}\sin(\theta_{ij}(t))]/\tau_{ij} \qquad \forall (i,j) \in \mathcal{L} \qquad (1n)$$
$$P_{ji}(t) = |V_j(t)|^2 g_{ij} - |V_i(t)||V_j(t)|[g_{ij}\cos(\theta_{ji}(t)) + b_{ij}\sin(\theta_{ji}(t))]/\tau_{ij} \qquad \forall (i,j) \in \mathcal{L} \qquad (1o)$$
$$Q_{ij}(t) = -|V_i(t)|^2(b_{ij} + \frac{b_{sh,ij}}{2})/\tau_{ij}^2 + |V_i(t)||V_j(t)| \cdot [b_{ij}\cos(\theta_{ij}(t)) - g_{ij}\sin(\theta_{ij}(t))]/\tau_{ij} \qquad \forall (i,j) \in \mathcal{L} \qquad (1p)$$
$$Q_{ji}(t) = -|V_j(t)|^2(b_{ij} + \frac{b_{sh,ij}}{2}) + |V_i(t)||V_j(t)| \cdot [b_{ij}\cos(\theta_{ji}(t)) - g_{ij}\sin(\theta_{ji}(t))]/\tau_{ij} \qquad \forall (i,j) \in \mathcal{L} \qquad (1q)$$
$$P_{ij}(t)^2 + Q_{ij}(t)^2 \leq \left(S_{ij}^{max}\right)^2 \qquad \forall (i,j) \in \mathcal{L} \qquad (1r)$$
$$P_{ji}(t)^2 + Q_{ji}(t)^2 \leq \left(S_{ij}^{max}\right)^2 \qquad \forall (i,j) \in \mathcal{L} \qquad (1s)$$
$$P_{g,i}(t) + P_{w,i}(t) + r_{d,i}(t) - r_{c,i}(t) - P_{d,i}(t) = \sum_{(i,j)\in\mathcal{L}} P_{ij}(t) + \sum_{(j,i)\in\mathcal{L}} P_{ij}(t) + g_{sh,i}|V_i(t)|^2 \qquad \forall i \in \mathcal{N} \qquad (1t)$$
$$Q_{g,i}(t) - Q_{d,i}(t) = \sum_{(i,j)\in\mathcal{L}} Q_{ij}(t) + \sum_{(j,i)\in\mathcal{L}} Q_{ij}(t) + b_{sh,i}|V_i(t)|^2 \qquad \forall i \in \mathcal{N} \qquad (1u)$$

where the power injections equal zero when the corresponding device does not exist at a bus (e.g., $P_{g,i} = 0, \forall i \in \mathcal{N}\backslash\mathcal{G}$). Constraints (1b) and (1c) limit the active and reactive generation at conventional generators. Constraint (1d) limits the active power output of wind generators. Constraints (1e) and (1f) limit the charge and discharge rates, respectively, (1g) limits the maximum energy storage, and (1j) controls the state-of-charge evolution with boundary conditions set by (1h) and (1i)[1]. Constraint (1k) prevents simultaneous charging and discharging of the storage devices. See [28] for further details on this storage device model.[2] The voltage magnitude limits are enforced by (1l), and (1m) sets the reference angle. Constraints (1n)-(1q) define the active and reactive line flows at both ends of each branch in the network, where for each line $(i,j) \in \mathcal{L}$, $\theta_{ij} = \theta_i - \theta_j - \theta_{shift,ij}$, and $\theta_{ji} = \theta_j - \theta_i + \theta_{shift,ij}$. These line flows are used in (1r)-(1s) to enforce apparent power line flow limits. The power flow equations (1t) and (1u) relate the voltages and the power injections. Note that adding generator ramp rate limits to this formulation is straightforward; these constraints are excluded for simplicity.

B. SOCP Relaxation of the Multiperiod OPF Problem

The multiperiod OPF problem in (1) is a non-convex optimization problem due to the nonlinear power flow equations (1t) and (1u) as well as the complementarity constraint (1k) that prevents simultaneous charging and discharging of the storage devices. This section addresses both sources of non-convexity to form a convex relaxation of (1).

1) SOCP Relaxation of the Power Flow Equations: Recent research efforts have developed a diverse variety of convex relaxations of the power flow equations, with trade-offs in computational tractability and tightness. In order to initialize the AC-QP algorithm, we desire a convex relaxation with fast computational speed. We have therefore selected the "branch-flow model" (BFM) relaxation of the power flow equations from [34]. The BFM relaxation has beneficial numerical characteristics relative to another SOCP relaxation based on a "bus-injection model" [35] and is faster than other convex relaxations based on semidefinite programming (e.g., [11], [12], [14], [18]).

The BFM approach in [34] relaxes the DistFlow equations [36], which formulate the power flow equations in terms of active power, reactive power, and squared current magnitude flows, $P_{ij}(t)$, $Q_{ij}(t)$, and $L_{ij}(t)$, respectively, out of terminal i for each line $(i,j) \in \mathcal{L}$ as well as squared voltage magnitudes $|V_i(t)|^2$ at each bus $i \in \mathcal{N}$ and time $t \in \mathcal{T}$. Note that we suppress the time dependence on the rest of the equations in this section for brevity.

To derive the BFM relaxation, we begin with the relationship between the active and reactive line flows and the squared current magnitude (see Fig. 1):

$$L_{ij}|V_i|^2 = (P_{ij})^2 + (Q_{ij})^2. \qquad (2)$$

To form an SOCP, (2) is relaxed to an inequality constraint:

$$L_{ij}|V_i|^2 \geq (P_{ij})^2 + (Q_{ij})^2. \qquad (3)$$

The current flow on the series impedance of the Π-circuit model is:

$$I_\pi = \left(\frac{P_{ij} - \mathbf{j}Q_{ij}}{\overline{V}_i}\right)\left(\tau_{ij}e^{-\mathbf{j}\theta_{shift,ij}}\right) - \mathbf{j}\frac{b_{sh,ij}V_i}{2\tau_{ij}e^{\mathbf{j}\theta_{shift,ij}}}. \qquad (4)$$

The relationship between the terminal voltages is:

$$\frac{V_i}{\tau_{ij}e^{\mathbf{j}\theta_{shift,ij}}} - I_\pi\left(R_{ij} + \mathbf{j}X_{ij}\right) = V_j. \qquad (5)$$

Taking the squared magnitude of both sides of (5) and using (2) and (4) yields:

$$|V_j|^2 = \frac{|V_i|^2}{\tau_{ij}^2} - 2\left(X_{ij}Q_{ij} + R_{ij}P_{ij}\right) - |V_i|^2 X_{ij}\frac{b_{sh,ij}}{\tau_{ij}^2} + \left(R_{ij}^2 + X_{ij}^2\right)\left(Q_{ij}b_{sh,ij} + \tau_{ij}^2 L_{ij} + \frac{b_{sh,ij}^2|V_i|^2}{4\tau_{ij}^2}\right). \qquad (6)$$

Active and reactive line losses are:

$$P_{loss,ij} = R_{ij}\tau_{ij}^2 L_{ij} + \frac{R_{ij}b_{sh,ij}^2}{4\tau_{ij}^2}|V_i|^2 + Q_{ij}R_{ij}b_{sh,ij} \qquad (7a)$$

$$Q_{loss,ij} = X_{ij}\tau_{ij}^2 L_{ij} + \Big(\frac{X_{ij}b_{sh,ij}^2 - 2b_{sh,ij}}{4\tau_{ij}^2}\Big)|V_i|^2. \qquad (7b)$$

The active and reactive injections at bus k are:

$$P_k^{SOCP} = \sum_{(k,j)\in\mathcal{L}} P_{kj} + \sum_{(i,k)\in\mathcal{L}}\left(P_{loss,ik} - P_{ik}\right) + g_{sh,k}|V_k|^2 \qquad (8a)$$

$$Q_k^{SOCP} = \sum_{(k,j)\in\mathcal{L}} Q_{kj} + \sum_{(i,k)\in\mathcal{L}}\left(Q_{loss,ik} - Q_{ik}\right) + b_{sh,k}|V_k|^2. \qquad (8b)$$

[1] Without constraint (1i) on the final state-of-charge, the optimization problem will typically use storage in a greedy manner, fully discharging the storage device to minimize operational cost within the time horizon. More details on the choice of e_i^{term} and its impact on solution quality can be found in [33].

[2] Constraints (1e)-(1k) could be replaced with another storage model if desired; the proposed framework is not limited to this modeling choice.

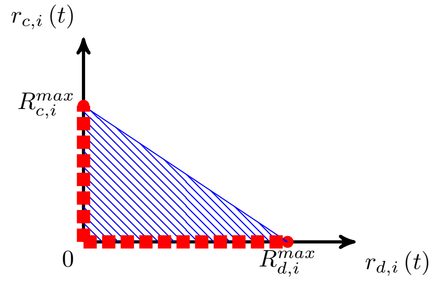

Fig. 2. Charging/discharging characteristic. The complementarity constraint (1k), with feasible space denoted by the red dashed lines, prevents simultaneous charging and discharging. The blue region shows the convex relaxation of the complementarity constraint (9) that is used in the SOCP relaxation.

2) Relaxation of the Charging/Discharging Complementarity Condition: The complementarity constraint (1k) prevents simultaneous charging and discharging of storage devices, which would lead to "fictitious" consumption of energy in devices with non-ideal efficiencies (i.e., $\eta_{c,i}, \eta_{d,i} < 1$). There are situations where simultaneous charging and discharging would reduce overall operating costs. In particular, such a cost reduction would be achieved by allowing simultaneous charging and discharging whenever a storage device was located at a bus with a negative "Locational Marginal Price" (i.e., a negative-valued Lagrange multiplier associated with the active power balance constraint (1t)). The constraint (1k) is therefore needed to ensure realistic storage device capabilities.

The feasible region for constraint (1k) is defined by the red dashed lines on the axes in Fig. 2. We use a convex relaxation of this space, which is given by the blue region in Fig. 2. Mathematically, this constraint is given by (1e) and (1f) augmented with:

$$r_{c,i}(t) \le -\Big(\frac{R_{c,i}^{max}}{R_{d,i}^{max}}\Big) r_{d,i}(t) + R_{c,i}^{max} \qquad \forall i \in \mathcal{S}, t \in \mathcal{T}. \quad (9)$$

While this formulation allows some degree of simultaneous charging and discharging (i.e., points in the blue region that are not on the red lines in Fig. 2), it is the most straightforward way to approximate the complementarity constraint. Other techniques for enforcing this constraint have been proposed, including modifying the OPF objective to include a cost for storage (dis)charging, which can be shown to strictly enforce complementarity under certain conditions [37], [38]. Since conditions resulting in simultaneous charging and discharging are relatively rare, the convex relaxation typically provides good initializations and close lower bounds, as demonstrated by the results in Section III.[3]

3) Formulation of the SOCP Relaxation of the Multiperiod OPF Problem: The SOCP relaxation of the multiperiod OPF problem is given by combining the relaxations of the power flow equations and the complementarity constraint:

$$\min \sum_{t\in\mathcal{T}}\sum_{i\in\mathcal{G}} \omega_i(t) \qquad \text{subject to } (\forall t \in \mathcal{T}) \qquad (10a)$$

Eqns. (1b)–(1j), (1m), (3), (7)–(9)

$$1 - c_{1,i}P_{g,i}(t) - c_{0,i} + \omega_i(t) \ge \left\| \begin{bmatrix} 1 + c_{1,i}P_{g,i}(t) + c_{0,i} - \omega_i(t) \\ 2\sqrt{c_{2,i}}\,P_{g,i}(t) \end{bmatrix} \right\|_2 \quad \forall i \in \mathcal{G} \quad (10b)$$

$$(V_i^{min})^2 \le |V_i(t)|^2 \le (V_i^{max})^2 \qquad \forall i \in \mathcal{N} \quad (10c)$$

$$S_{ij}^{max} \ge \left\| \begin{bmatrix} P_{ij}(t) \\ Q_{ij}(t) \end{bmatrix} \right\|_2 \qquad \forall (i,j) \in \mathcal{L} \quad (10d)$$

$$S_{ij}^{max} \ge \left\| \begin{bmatrix} P_{loss,ij}(t) - P_{ij}(t) \\ Q_{loss,ij}(t) - Q_{ij}(t) \end{bmatrix} \right\|_2 \qquad \forall (i,j) \in \mathcal{L} \quad (10e)$$

$$P_{g,i}(t) + P_{w,i}(t) + r_{d,i}(t) - r_{c,i}(t) - P_{d,i}(t) = P_i^{SOCP}(t) \qquad \forall i \in \mathcal{N} \quad (10f)$$

$$Q_{g,i}(t) - Q_{d,i}(t) = Q_i^{SOCP}(t) \qquad \forall i \in \mathcal{N} \quad (10g)$$

where $\|\cdot\|_2$ denotes the two-norm. Note that the line-flow limits (10d)–(10e) and the squared current equation (3) are implemented with second-order cone constraints. The quadratic objective is implemented with the auxiliary variables $\omega_i(t)$, $i \in \mathcal{G}$, $t \in \mathcal{T}$ and the SOCP constraint (10b). The remainder of the constraints are linear. Thus, (10) is an SOCP.

Without consideration of the complementarity constraint (1k), the SOCP relaxation is *exact* (i.e., yields the globally optimal solution) for radial networks that satisfy certain non-trivial technical conditions [34]. However, for more general networks such as those considered in this paper, the relaxation is usually not exact. Nevertheless, the SOCP relaxation (10) lower bounds the optimal objective value of (1) and, as will be shown in the following sections, often provides a good initialization for an AC-QP algorithm in the following manner. The SOCP solution provides the power injections $P_g(t)$, $Q_g(t)$, $P_w(t)$, $r_c(t)$, $r_d(t)$ and voltage magnitudes (implied by $\sqrt{|V_i(t)|^2}$) that are used for the initial power flow. Additionally, voltage angle differences across each line in the network are calculated from the apparent power line flows and voltage magnitudes. Based on those angle differences, a least-squares problem then establishes a best fit for the voltage angles at all nodes in the network. This provides an initialization for voltage angles. The voltage magnitude and angle schedules from the SOCP initialization are particularly useful when applying the AC-QP algorithm to large systems, where obtaining a converged AC power flow can be challenging.

C. AC-QP OPF Algorithm

We next describe the AC-QP OPF algorithm, a local solution method adopted from [1], which is summarized in Fig. 3. The successive linearization procedure in this method often benefits greatly from initialization near the global optimum. In the AC-QP algorithm, an AC power flow is first solved from an initial approximate operating point. This provides the Jacobian of the power flow equations, $\mathbf{J}(t)$, as well as the line-flow sensitivity factors $\frac{\partial S_{ij}}{\partial \theta_k}(t)$ and $\frac{\partial S_{ij}}{\partial |V_k|}(t)$ at each time $t \in \mathcal{T}$. A QP is then solved to find a generation schedule that minimizes the generation cost while enforcing (linearized) power balance equations. The QP solution provides new generation and voltage schedules that are used in the next set[4] of AC power flows.

The initial (dis)charging status of each storage device $i \in \mathcal{S}$ at each time step $t \in \mathcal{T}$ is determined by the net value of

[3]The complementarity constraint is enforced in the AC-QP algorithm, so the final solution cannot have simultaneous charging and discharging.

[4]A separate power flow is required for each time step.

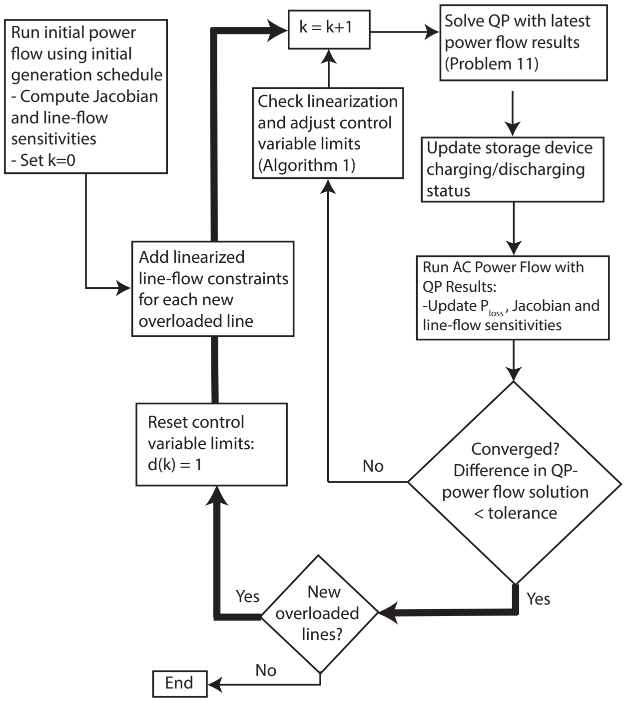

Fig. 3. Flowchart for the AC-QP OPF algorithm, (adapted from [1], [39]).

charging/discharging given by the SOCP. When in charging mode, the status is enforced in the QP by setting the discharging limit $R_{d,i}^{max}(t)$ to zero, with $R_{c,i}^{max}(t)$ taking its proper value. If the QP solves to a non-zero value of $r_{c,i}(t)$, the status remains unchanged for the next AC-QP iteration. If, however, the QP solves to the zero limit $r_{c,i}(t) = 0$ and the Lagrangian multiplier corresponding to that lower inequality constraint is positive[5] then the status is changed to discharging for the next iteration of the AC-QP algorithm. Likewise for transitioning from discharging to charging. Thus, constraint (1k) is enforced in a iterative manner. A more detailed discussion of this process can be found in [40].

The QP–(power flow) iterations continue until the difference between the QP and power flow solutions agrees to within a specified tolerance (10^{-3} pu provides sufficient accuracy). At that point, the inner loop of the method is terminated.

In the QP, the notation Δ is used to denote a change in the corresponding variable at the current iteration of the AC-QP algorithm. The superscript '$\circ$' denotes values obtained from the AC power flow. These are updated after each QP–(power flow) iteration. The QP solved at each iteration makes use of the power flow linearization:

$$\mathbf{J}(t) = \begin{bmatrix} \frac{\partial P}{\partial \theta}(t) & \frac{\partial P}{\partial |V|}(t) \\ \frac{\partial Q}{\partial \theta}(t) & \frac{\partial Q}{\partial |V|}(t) \end{bmatrix}, \qquad \Delta x(t) = \begin{bmatrix} \Delta\theta(t) \\ \Delta|V(t)| \end{bmatrix}$$

$$\Delta S(t) = \begin{bmatrix} \Delta P_g(t) - \Delta r_c(t) + \Delta r_d(t) + \Delta P_w(t) \\ \Delta Q_g(t) \end{bmatrix}$$

and is formulated as:

$$\min \sum_{t\in\mathcal{T}} \sum_{i\in\mathcal{G}} C_i\big(P_{g,i}^{\circ}(t) + \Delta P_{g,i}(t)\big) \quad \text{subject to } (\forall t \in \mathcal{T}) \tag{11a}$$

$$\mathbf{J}(t)\Delta x(t) = \Delta S(t) \tag{11b}$$

$$P_{g,i}^{min} \le P_{g,i}^{\circ}(t) + \Delta P_{g,i}(t) \le P_{g,i}^{max} \qquad \forall i \in \mathcal{G} \tag{11c}$$

$$Q_{g,i}^{min} \le Q_{g,i}^{\circ}(t) + \Delta Q_{g,i}(t) \le Q_{g,i}^{max} \qquad \forall i \in \mathcal{G} \tag{11d}$$

$$\Delta\theta_{slack}(t) = 0 \tag{11e}$$

$$-\pi \le \theta_i^{\circ}(t) + \Delta\theta_i(t) \le \pi \qquad \forall i \in \mathcal{N}\backslash slack \tag{11f}$$

$$V_i^{min} \le |V_i^{\circ}(t)| + \Delta|V_i(t)| \le V_i^{max} \qquad \forall i \in \mathcal{N} \tag{11g}$$

$$0 \le P_{w,i}^{\circ}(t) + \Delta P_{w,i}(t) \le W_i^{max}(t) \qquad \forall i \in \mathcal{W} \tag{11h}$$

$$\begin{aligned} T_s \left(\eta_c \left(r_{c,i}^{\circ}(t) + \Delta r_{c,i}(t)\right) - \left(r_{d,i}^{\circ}(t) + \Delta r_{d,i}(t)\right)/\eta_{d,i}\right) \\ = e_i(t+1) - e_i(t) \qquad \forall i \in \mathcal{S} \end{aligned} \tag{11i}$$

$$e_i(0) = e_i^{init} \qquad \forall i \in \mathcal{S} \tag{11j}$$

$$e_i(T) = e_i^{term} \qquad \forall i \in \mathcal{S} \tag{11k}$$

$$0 \le r_{c,i}^{\circ}(t) + \Delta r_{c,i}(t) \le R_{c,i}^{max}(t) \qquad \forall i \in \mathcal{S} \tag{11l}$$

$$0 \le r_{d,i}^{\circ}(t) + \Delta r_{d,i}(t) \le R_{d,i}^{max}(t) \qquad \forall i \in \mathcal{S} \tag{11m}$$

$$0 \le e_i(t) \le E_i \qquad \forall i \in \mathcal{S} \tag{11n}$$

$$\begin{aligned} S_{ij}^{\circ}(t) + \sum_{k\in\mathcal{N}} \frac{\partial S_{ij}}{\partial \theta_k}(t)\Delta\theta_k(t) + \sum_{k\in\mathcal{N}} \frac{\partial S_{ij}}{\partial |V_k(t)|}\Delta|V_k(t)| \le S_{ij}^{max} \\ \forall\, (i,j) \in \mathcal{L}^* \end{aligned} \tag{11o}$$

$$\begin{aligned} S_{ji}^{\circ}(t) + \sum_{k\in\mathcal{N}} \frac{\partial S_{ji}}{\partial \theta_k}(t)\Delta\theta_k(t) + \sum_{k\in\mathcal{N}} \frac{\partial S_{ji}}{\partial |V_k(t)|}\Delta|V_k(t)| \le S_{ij}^{max} \\ \forall\, (i,j) \in \mathcal{L}^* \end{aligned} \tag{11p}$$

where the linearized line-flow constraints (11o)-(11p) are enforced for all lines that are at or above 95% of their line-flow limit, the set of which is denoted $\mathcal{L}^*$. This set is updated at the beginning of each outer loop of the AC-QP algorithm (bolded in Fig. 3). Constraints (11i)–(11n) model the storage state-of-charge dynamics with non-ideal charging and discharging efficiencies.

The convergence of this method depends on the accuracy of the linearization at each iteration. To improve convergence, a "trust-region" step, based on the formulation in [39], is added to check the accuracy of the linearization before the next QP is solved. The implementation of the trust-region step is summarized in Algorithm 1.

The actual change in the total losses,

$$\Delta P_{loss\_act}^{k}(t) = P_{loss}^{k}(t) - P_{loss}^{k-1}(t), \qquad \forall t \in \mathcal{T}, \tag{12}$$

is computed after the power flow step, where superscript k indicates the k^{th} iteration of the AC-QP algorithm. The actual change in losses is compared with that predicted from the QP solution,

$$\begin{aligned} &\Delta P_{loss\_pred}^{k}(t) = \\ &\sum_{i\in\mathcal{N}} \sum_{j\in\mathcal{N}} \left[\left(\frac{\partial P_i}{\partial \theta_j}(t)\right)^{k-1} \Delta\theta_j^k(t) + \left(\frac{\partial P_i}{\partial |V_j|}(t)\right)^{k-1} \Delta|V_j(t)|^k \right]. \end{aligned} \tag{13}$$

If the difference between the predicted and actual losses at each time $t \in \mathcal{T}$ is within a specified tolerance (a suitable value being 10%), the linearization is considered sufficiently accurate. Otherwise, the linearization is of questionable accuracy, and all control variable limits in the QP at the next iteration are reduced by a scaling factor, denoted $d(k)$ for iteration k. If after the next QP–(power flow) iteration the linearization is again insufficiently accurate, the scaling factor $d(k)$ is further reduced by a constant, denoted Sc in Algorithm 1. (A value of $Sc = 0.5$ was used in our implementation.) If

[5] A positive Lagrangian multiplier indicates that the cost would be reduced by moving beyond the limit.

Algorithm 1 Trust-region step of the AC-QP OPF algorithm

Calculate the predicted change in system losses from the QP solution at each time $t \in \mathcal{T}$ according to (13).
Calculate the actual change in system losses from the power flow solution at each time $t \in \mathcal{T}$ according to (12).
Update QP control variable limits at the next iteration:
if $\max_{t\in\mathcal{T}} |\Delta P^k_{loss\_act}(t) - \Delta P^k_{loss\_pred}(t)| <$ tolerance
    The linearization is considered accurate.
    Increase control variable limits at next iteration by a scaling factor: $d(k+1) = \min(2 \times d(k), 1)$.
else
    The linearization is considered inaccurate.
    Reduce control variable limits at next iteration by a scaling factor: $d(k+1) = Sc \times d(k)$.
end if

the linearization provides acceptable accuracy though, $d(k)$ is increased according to $d(k+1) = \min(2 \times d(k), 1)$.

This process reduces the magnitude of the changes from the previous AC power flow solution that can be scheduled by the QP. As the control variable step size at each iteration shrinks until the linearization is sufficiently accurate, this improves the convergence of the inner loop of the method. If the outer loop is required because new lines become overloaded, control variable limits are reset to their original values (i.e. $d(k) = 1$) and the process repeats.

Often convergence can be further improved by reducing the range of values that appear in the admittance matrix. This is achieved by removing low-impedance lines (i.e., lines with impedance less than 1×10^{-3} pu) by merging the connected buses using the method described in [41]. This is similar to the preprocessing steps used in many commercial software packages, for example [42].

III. Results and Discussion

Both the SOCP relaxation and AC-QP algorithm have been applied to a variety of test cases. This section presents detailed results for two of these test cases: modified versions of the Polish 3012wp test case [43] and a 30-bus loop network [44]. The scalability of these methods is further demonstrated using five other large test cases (the Polish 2383wp, 2737sop and 3120sp cases [43], the 2869-bus PEGASE network representing portions of the European power system [45], and a 4259-bus model of the Californian region of WECC). A summary of the test case details is provided in Table I.

It has been observed that for large-scale networks and a time horizon exceeding 16 time steps, the AC-QP OPF is likely to require solution times longer than 5 minutes, which is a reasonable time limit for on-line applications. Moreover, it was shown in [33] that a moderate horizon of 4 hours (8 step with $T_s = 30$ minutes) was sufficient to obtain the economic benefits of operating storage with renewable generation. All test cases therefore consider a horizon of 4 hours with a time-step of $T_s = 30$ minutes, for a total of 8 time steps. Because renewable generation may change more rapidly than this 30-minute time step, in an operational setting this algorithm could be re-run frequently (every 5 to 10 minutes) using a receding horizon strategy [46] to account for deviations in measured and forecast generation.

TABLE I
Descriptions of Test Cases

Test Network	Number of Buses, Lines	Number Wind Buses	Number Storage Buses	Renewable Penetration (%)
PL-3012wp	2292, 2851	70	300	8.4
30-bus loop	30, 30	5	3	0.0049
PL-2383wp	2177, 2690	60	238	7.3
PEGASE-2869	2487, 4164	70	287	1.3
PL-3120sp	2314, 2886	70	312	10.0
PL-2737sop	2183, 2715	35	274	12.2
WECC	4259, 5868	531	10	45.2

Storage and wind generation were added to each test network at randomly chosen buses. As the focus of this work is to provide an improved initialization for the AC-QP OPF method, the purpose of adding storage and wind in these cases is to exercise the multiperiod OPF formulation. The available wind $W_i^{max}(t)$ at each wind bus was chosen from a uniform random distribution over the range 1 to 100 MW. The corresponding renewable penetration of each test case, which is calculated as the total available wind generation as a percentage of total conventional generation capacity, is given in the final column of Table I. This forecast of available wind at each location is assumed to be perfect, as this work relies upon a deterministic OPF formulation.[6] Storage device power ratings were chosen from a uniform distribution of 1–5 MW, and storage device energy ratings were chosen from a uniform distribution of 1–20 MWh. Table I provides additional details for these test cases.

Three initialization approaches for the AC-QP algorithm were tested. The first used the generation and voltage schedules provided in the test case description. With this method, storage and wind are unused in the initialization (i.e., no charging or discharging and full wind curtailment). The second is a DC OPF that approximates total system losses as 3% of total load (i.e., the DC power balance constraint at each bus is modified to include an additional 3% of the demand and storage charging at that bus to account for system losses). The final initialization method is the SOCP relaxation.[7]

The formulations were implemented in MATLAB R2012a and solved on a MacBook Pro with a quad-core Intel i7 2.3 GHz processor with 16 GB of 1600 MHz DDR3 RAM using MOSEK version 7.0 to solve the SOCP programs and Gurobi version 5.6.3 to solve the quadratic programs. A Newton algorithm was used to solve the power flows.

[6] As mentioned earlier, the deterministic OPF can be embedded in a receding horizon strategy to account for variability and uncertainty. Furthermore, such deterministic OPF problems form the basis of many stochastic OPF formulations. Integrating the proposed approach into stochastic OPF methods is discussed as future work in Section IV.

[7] In an on-line environment, the state estimator solution would be available to initialize the OPF. As a surrogate, we also considered an initialization based on the single-time-step OPF solution at $t = 0$, copied to each later time step. The results indicated that this approach was generally inferior to the initialization from the SOCP relaxation in both computation time and solution quality. Inferiority of the single-step initialization is attributable to the fact that it does not consider the forecast of future wind availability and the corresponding changes in storage utilization, both of which are available to other initialization methods.

TABLE II
PL-3012WP: EXPLICITLY ENFORCED LINE-FLOW CONSTRAINTS

Initialization Method	Initial Lines (Additional Lines)	Line Limits Binding at Soln.
Case description	324, 331, 529, 813, 1411, 1412, 1436, 1833, 2225, (231), (495), (1367), (1388), (1519), (2829)	231, 495, 529, 1367, 1388, 1519, (2829)
DC OPF	231, 495, 542, 813, 1367, 1388, 1519, 1718, 1833, 1878, 2233, 2473, 2608, 2829, (529)	231, 495, (529), 1367, 1388, 1519, 2829
SOCP	231, 495, 529, 542, 813, 1367, 1388, 1519, 1833, 2233, 2473, 2829	231, 495, 529, 1367, 1388, 1519, 2829

TABLE III
PL-3012WP: CONVERGENCE AND EXECUTION TIME

Initialization Method	Number of QP–(power flow) iterations	Init. Time (sec)	AC-QP Time (sec)	Total Time (sec)
Case Description	7	–	111	111
DC OPF	7	18	107	124
SOCP	4	19	58	77

The results in this section demonstrate the computational tractability and solution quality for the proposed approach of using the SOCP initialization with the AC-QP algorithm.

A. Case 1: Polish 3012wp Network

The convergence and computation time of the AC-QP algorithm are substantially improved by accurately predicting which line-flow constraints need to be explicitly enforced in the QP (i.e., determining the set $\mathcal{L}^*$). The initial set of line-flow constraints is highly dependent on the choice of initialization. This first test case emphasizes an important benefit of the SOCP initialization method: compared to the other initializations, the power flow solution resulting from the SOCP initialization more accurately predicts the set of line-flow constraints that must be included in the QP. Consequently, fewer outer loops of the AC-QP algorithm (the bold path in Fig. 3) are required, reducing the number of QP–(power flow) iterations and hence the computation time.

The results of the Polish 3012wp test case are summarized in Tables II–III. For each initialization method, the second column of Table II gives the line index for line-flow constraints that are added to the QP. The lines shown in parentheses were not identified from the initial power flow, but were added through additional outer loops as they became overloaded in subsequent iterations of the AC-QP algorithm. Compared with the other methods, the SOCP initialization performs better in two aspects: 1) it requires the fewest number of explicitly enforced line-flow constraints, which reduces the time required to solve the QP at each iteration, and 2) the initial set of line-flow constraints is sufficient throughout the AC-QP iterations (i.e., no additional outer loops of the AC-QP algorithm are required). The third column of Table II demonstrates that regardless of the initialization procedure, the same line constraints are binding in the final solution for this test case. Only the SOCP initialization yields a superset of the binding line-flow constraints.

Table III indicates that the SOCP initialization offers appreciable performance improvements over the other forms of initialization. The SOCP method eliminates the need for additional outer loops to add line-flow constraints not initially identified, thus reducing the total number of iterations, as shown in the second column. Explicitly enforcing fewer inequality constraints reduces the QP's solution time at each iteration. These two factors greatly reduce the solution time of the AC-QP algorithm, as demonstrated in the fourth column of this table. The fifth column shows that SOCP initialization results in a total computation time that is substantially less than the other methods. These timing results also highlight the scalability of these methods for large networks.

The objective value of the SOCP relaxation lower bounds the generation cost, thus providing a useful metric for assessing the quality of the solution obtained from the AC-QP algorithm. For this example, the SOCP gave a lower bound of 13.602 M$ on the cost of generation. All three initialization processes resulted in convergence to the same total cost of generation of 13.618 M$, implying a relaxation gap of at most 0.12%. Thus, the AC-QP solution is at least very close to being globally optimal, and may, in fact, be the global optimum.[8] Even though all initialization methods resulted in equivalent dispatches, the choice of initialization process significantly affected the solution time and the number of iterations required to reach that solution.

B. Case 2: 30-Bus Loop Network

The SOCP initialization is also useful for cases where the AC-QP algorithm finds a local solution rather than the global optimum. The AC-QP algorithm provides neither a guarantee of finding a global solution nor a metric for assessing solution quality. As shown in [44], OPF problems may have multiple locally optimal solutions. Tables IV–V provide results for a modified multiperiod version of the 30-bus loop test case from [44] that demonstrate the utility of the SOCP initialization for both finding a global solution and providing a metric of solution quality.

As shown in Table IV, initializing the AC-QP algorithm using the case description or the DC OPF results in solution costs that are significantly higher than the SOCP lower bound, while the SOCP initialization gives a cost that is within 0.0011% of the lower bound.[9] Using the lower bound from the SOCP relaxation as an indicator of solution quality, it is reasonable to assert that the solution resulting from the SOCP initialization is sufficiently close to the global optimum, while the other two solutions are locally optimal solutions.

In this example, the suboptimal solutions resulting from the DC OPF and case description initializations have power circulating around the loop while the global solution does not. As shown in Table V, this circulating power results in greatly

[8]This gap can be at least partially attributed to relaxations of the power flow equations (10f),(10g) and the simultaneous charging/discharging constraint (9). For several test cases, solutions to the relaxation (10) exhibited simultaneous charging and discharging at some buses.

[9]The SOCP relaxation does not always yield a lower bound that is close to the global optimum (e.g., the lower bound from the SOCP relaxation of the nine-bus system in [44] is 11% below the global optimum identified in [15]).

TABLE IV
30-BUS LOOP: GENERATION COST

Initialization Method	SOCP Lower Bound ($)	AC-QP Cost ($)	% Cost Difference
Case description	23,840	31,577	32.5 %
DC OPF	23,840	26,759	12.2 %
SOCP	23,840	23,840	0.0011 %

TABLE V
30-BUS LOOP: TOTAL GENERATION AND LOSSES

Initialization Method	AC-QP Total Generation (MW)	AC-QP Total Losses (MW)
Case description	15,788	3,937.5
DC OPF	13,380	1,526.5
SOCP	11,920	69.3

increased losses. Substantially more generation is required, incurring higher cost. Moreover, as each branch has a relatively small angle difference, identifying such local optima may be difficult in more general problems. Similar phenomena have been observed in actual systems, as described in [47].

The example demonstrates the value of the SOCP relaxation: 1) it provides a sufficient condition for quickly assessing whether a solution to the AC-QP algorithm has an objective value that is close to the globally optimal value, and 2) SOCP initialization results in a globally optimal solution for this case.

C. Other Large Test Cases

The AC-QP algorithm with its various initializations was also applied to other large test cases, including a 4259-bus model of the WECC system, to assess performance on networks of various sizes and topologies. An 8-step time horizon was used in all cases. The details of these test cases are given in Table I, and the results are summarized in Tables VI–IX. Tables VI and VII show the convergence results of each test case and each initialization method. In each case, the SOCP initialization method improves the convergence rate of the AC-QP algorithm, requiring a smaller number of iterations and achieving the fastest total execution time. The computational improvement is particularly significant for the PEGASE-2869 and PL-3120sp test cases. It is important to note that these execution time improvements are achieved by changing only the initialization procedure.

Initialization of the WECC case is particularly challenging. The initial power flow of the AC-QP algorithm did not converge when initialized using the case description or the DC OPF. This resulted in failure of the AC-QP algorithm. In contrast, SOCP initialization provides close-to-feasible initial conditions that result in convergence of the initial power flow (and subsequently of the AC-QP algorithm). Note that the execution time for the WECC case is fast enough for use in a practical on-line setting, although including other features, such as contingency constraints, requires further work.

Table VIII gives the total cost of generation while Table IX provides the corresponding percent difference in generation cost between the lower bound of the SOCP relaxation and the AC-QP solution. In all cases, the SOCP initialization yields the AC-QP solution with generation cost closest to the SOCP

TABLE VI
NUMBER OF ITERATIONS FOR TEST CASES

Test Network	Case Description Init.	DC-OPF Init.	SOCP Init.
PL-2383wp	8	5	5
PEGASE-2869	8	8	4
PL-3120sp	11	7	5
PL-2737sop	6	6	3
WECC	–	–	4

TABLE VII
TOTAL EXECUTION TIME (SECONDS) FOR TEST CASES

Test Network	Case Description Init.	DC-OPF Init.	SOCP Init.
PL-2383wp	97	77	78
PEGASE-2869	127	149	87
PL-3120sp	159	126	98
PL-2737sop	81	94	62
WECC	–	–	128

TABLE VIII
TOTAL COST OF GENERATION FOR TEST CASES

Test Network	SOCP Lower Bound (M$)	Case Description Init. (M$)	DC-OPF Init. (M$)	SOCP Init. (M$)
PL-2383wp	8.58	8.61	8.65	8.60
PEGASE-2869	0.875	0.882	0.879	0.878
PL-3120sp	11.2	11.2	11.2	11.2
PL-2737sop	6.44	6.47	6.47	6.47
WECC	0.208	–	–	0.208

lower bound. It therefore provides a more economic operating point than those resulting from the other two initializations. We note, however, that the small differences in Table IX may be due in part to the termination criterion used in the AC-QP algorithm.

The case PL-2383wp is of particular interest due to larger cost variations among the different initialization methods. Fig. 4 shows the total storage (dis)charging across all storage devices, as well as the total wind generation across all wind nodes at each time step in the OPF horizon. Taking the AC-QP solution initialized with the SOCP as a reference, the results presented are normalized to show the difference in each solution for the various initialization algorithms. Looking at the storage (dis)charging results over the 8-step horizon, the solution from the DC OPF initialization generally makes less use of storage. As a consequence, less wind generation can be used to meet demand, resulting in higher cost of operation. This highlights the economic value of optimally scheduling storage in conjunction with renewable generation.

IV. CONCLUSIONS

The paper presents an OPF solution process that uses an SOCP relaxation to initialize an AC-QP successive linearization algorithm. The SOCP provides initial values for the decision variables (traditional and renewable generation, and energy storage charge/discharge values) along with approximate values for all voltage magnitudes and angles across the network. These values are particularly useful for achieving

TABLE IX
PERCENT COST DIFFERENCE (%) FOR TEST CASES

Test Network	Case Description Init.	DC-OPF Init.	SOCP Init.
PL-2383wp	0.40	0.82	0.23
PEGASE-2869	0.72	0.43	0.27
PL-3120sp	0.30	0.30	0.30
PL-2737sop	0.37	0.37	0.37
WECC	–	–	0.03

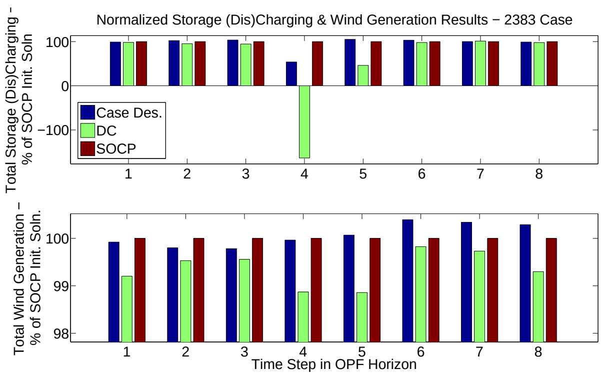

Fig. 4. An example of differing use of storage and wind resulting in local minima.

convergence of the initial power flow in the AC-QP algorithm. The resulting initial solution often lies in the vicinity of the globally optimal solution.

SOCP initialization offers several benefits over other approaches. The SOCP relaxation often provides an accurate prediction of the subset of line-flow constraints that require explicit representation in the QP. This reduces both the total number of iterations needed in the AC-QP algorithm as well as the number of inequality constraints in the QP. These factors improve the solution time of the AC-QP algorithm. The SOCP initialization reduces the likelihood of the AC-QP algorithm converging to a local optimum that is far from the global solution. Furthermore, the lower bound on the OPF objective given by the SOCP relaxation provides an indication of the quality of the AC-QP solution. A small "gap" between the SOCP lower bound and the AC-QP solution indicates that a nearly globally optimal outcome has been achieved.

The algorithm has been applied to a variety of multi-period OPF test cases that incorporate wind and storage resources. The results indicate that this approach scales well, with tractability demonstrated for large-scale test cases up to 4259 buses and 8 time-steps.

The proposed method motivates several research directions. The first is to explore initializing multiperiod OPF problems using other recently developed linear and SOCP relaxations and approximations of the power flow equations, such as those in [19], [20], [35], [48], [49]. Another direction is to include wind and/or demand uncertainty into the OPF problem. Some recent techniques for addressing uncertainty include adding a heuristically chosen set of scenarios to the OPF problem [50]–[52], assuming a closed-form uncertainty distribution to analytically reformulate the OPF problem [53], [54], and scenario approaches that offer performance guarantees [55], [56]. These methods rely upon solving modified deterministic OPF subproblems so the proposed AC-QP method is directly applicable. Furthermore, this work demonstrates that the SOCP relaxation provides useful results when applied to several meshed networks, though no theoretical guarantee as to its exactness exists. This observation merits further investigation. Finally, the computational performance of the SOCP-initialized AC-QP method enables thorough evaluation of the economic impact of renewable generation and energy storage in large-scale systems.

REFERENCES

[1] A. Wood, B. Wollenberg, and G. Sheble, *Power Generation, Operation and Control*, 3rd ed. John Wiley and Sons, Inc., 2013.

[2] M. Huneault and F. Galiana, "A Survey of the Optimal Power Flow Literature," *IEEE Trans. Power Syst.*, vol. 6, no. 2, pp. 762–770, May 1991.

[3] J. Momoh, R. Adapa, and M. El-Hawary, "A Review of Selected Optimal Power Flow Literature to 1993. Parts I & II," *IEEE Trans. Power Syst.*, vol. 14, no. 1, pp. 96–111, Feb. 1999.

[4] A. Castillo and R. O'Neill, "Survey of Approaches to Solving the ACOPF (OPF Paper 4)," US Federal Energy Regulatory Commission, Tech. Rep., Mar. 2013.

[5] A. Motto, F. Galiana, A. Conejo, and J. Arroyo, "Network-Constrained Multiperiod Auction for a Pool-Based Electricity Market," *IEEE Trans. Power Syst.*, vol. 17, no. 3, pp. 646–653, Aug. 2002.

[6] T. Overbye, X. Cheng, and Y. Sun, "A Comparison of the AC and DC Power Flow Model for LMP Calculations," in *37th Hawaii Int. Conf. Syst. Sci. (HICSS)*, Jan. 2006.

[7] M. Amini, R. Jaddivada, S. Mishra, and O. Karabasoglu, "Distributed Security Constrained Economic Dispatch," in *IEEE Innovative Smart Grid Technologies Conference (ISGT)*, Bangkok, Thailand, Nov. 2015.

[8] K. Purchala, L. Meeus, D. Van Dommelen, and R. Belmans, "Usefulness of DC Power Flow for Active Power Flow Analysis," *IEEE PES General Meeting*, pp. 454–459, June 2005.

[9] B. Stott, J. Jardim, and O. Alsac, "DC Power Flow Revisited," *IEEE Trans. Power Syst.*, vol. 24, no. 3, pp. 1290–1300, Aug. 2009.

[10] K. Dvijotham and D. Molzahn, "Error Bounds on Linear Power Flow Approximations: A Convex Relaxation Approach," in *IEEE 55th Annu. Conf. Decis. Control (CDC)*, Dec. 2016.

[11] X. Bai, H. Wei, K. Fujisawa, and Y. Wang, "Semidefinite Programming for Optimal Power Flow Problems," *Int. J. Electr. Power Energy Syst.*, vol. 30, no. 6, pp. 383–392, Feb. 2008.

[12] J. Lavaei and S. Low, "Zero Duality Gap in Optimal Power Flow Problem," *IEEE Trans. Power Syst.*, vol. 27, no. 1, pp. 92–107, Feb. 2012.

[13] S. Low, "Convex Relaxation of Optimal Power Flow–Part I: Formulations and Equivalence," *IEEE Trans. Control Netw. Syst.*, vol. 1, no. 1, pp. 15–27, Mar. 2014.

[14] D. Molzahn, J. Holzer, B. Lesieutre, and C. DeMarco, "Implementation of a Large-Scale Optimal Power Flow Solver Based on Semidefinite Programming," *IEEE Trans. Power Syst.*, vol. 28, no. 4, pp. 3987–3998, Nov. 2013.

[15] D. Molzahn and I. Hiskens, "Moment-Based Relaxation of the Optimal Power Flow Problem," *18th Power Syst. Comput. Conf. (PSCC)*, 18-22 Aug. 2014.

[16] B. Ghaddar, J. Marecek, and M. Mevissen, "Optimal Power Flow as a Polynomial Optimization Problem," *IEEE Trans. Power Syst.*, vol. 31, no. 1, pp. 539–546, Jan. 2016.

[17] C. Josz, J. Maeght, P. Panciatici, and J. Gilbert, "Application of the Moment-SOS Approach to Global Optimization of the OPF Problem," *IEEE Trans. Power Syst.*, vol. 30, no. 1, pp. 463–470, Jan. 2015.

[18] D. Molzahn and I. Hiskens, "Sparsity-Exploiting Moment-Based Relaxations of the Optimal Power Flow Problem," *IEEE Trans. Power Syst.*, vol. 30, no. 6, pp. 3168–3180, Nov. 2015.

[19] B. Kocuk, S. Dey, and A. Sun, "Strong SOCP Relaxations of the Optimal Power Flow Problem," To appear in *Oper. Res.*, 2015, arXiv:1504.06770.

[20] C. Coffrin, H. Hijazi, and P. Van Hentenryck, "The QC Relaxation: Theoretical and Computational Results on Optimal Power Flow," *IEEE Trans. Power Syst.*, vol. 31, no. 4, pp. 3008–3018, July 2016.

[21] E. Dall'Anese, H. Zhu, and G. Giannakis, "Distributed Optimal Power Flow for Smart Microgrids," *IEEE Trans. Smart Grid*, vol. 4, no. 3, pp. 1464–1475, Sept. 2013.

[22] D. Molzahn and I. Hiskens, "Mixed SDP/SOCP Moment Relaxations of the Optimal Power Flow Problem," in *IEEE Eindhoven PowerTech*, June 2015.

[23] R. Madani, S. Sojoudi, and J. Lavaei, "Convex Relaxation for Optimal Power Flow Problem: Mesh Networks," *IEEE Trans. on Power Systems*, vol. 30, no. 1, pp. 199–211, Jan. 2015.

[24] B. Lesieutre, D. Molzahn, A. Borden, and C. DeMarco, "Examining the Limits of the Application of Semidefinite Programming to Power Flow Problems," in *49th Annu. Allerton Conf. Commun., Control, Comput.*, Sept. 2011, pp. 1492–1499.

[25] D. Molzahn, B. Lesieutre, and C. DeMarco, "Investigation of Non-Zero Duality Gap Solutions to a Semidefinite Relaxation of the Optimal Power Flow Problem," in *47th Hawaii Int. Conf. Syst. Sci. (HICSS)*, 6-9 Jan. 2014.

[26] D. Molzahn and I. Hiskens, "Convex Relaxations of Optimal Power Flow Problems: An Illustrative Example," *IEEE Trans. Circuits Syst. I: Reg. Papers*, vol. 63, no. 5, pp. 650–660, May 2016.

[27] K. Chandy, S. Low, U. Topcu, and H. Xu, "A Simple Optimal Power Flow Model with Energy Storage," in *IEEE 49th Ann. Conf. Decis. Contr. (CDC)*, Atlanta, GA, Dec. 2010, pp. 1051–1057.

[28] M. Almassalkhi and I. Hiskens, "Cascade Mitigation in Energy Hub Networks," in *IEEE 50th Ann. Conf. Decis. Contr. (CDC)*, Orlando, FL, Dec. 2011, pp. 2181–2188.

[29] R. Jabr, S. Karaki, and J. Korbane, "Robust Multi-Period OPF With Storage and Renewables," *IEEE Trans. Power Syst.*, vol. 30, no. 5, pp. 2790–2799, September 2015.

[30] N. Nguyen, D. Bovo, and A. Berizzi, "Optimal Power Flow with Energy Storage Systems: Single-Period Model vs. Multi-Period Model," in *IEEE Eindhoven PowerTech*, June 2015.

[31] D. Gayme and U. Topcu, "Optimal Power Flow with Large-Scale Storage Integration," *IEEE Trans. Power Syst.*, vol. 28, no. 2, pp. 709–717, May 2013.

[32] A. Gopalakrishnan, A. U. Raghunathan, D. Nikovski, and L. T. Biegler, "Global Optimization of Multi-Period Optimal Power Flow," in *American Control Conference (ACC)*, Washington, DC, June 2013.

[33] J. Marley and I. Hiskens, "Multi-period AC-QP Optimal Power Flow Including Storage," in *19th Power Syst. Comput. Conf. (PSCC)*, June 2016.

[34] S. Low, "Convex Relaxation of Optimal Power Flow: Parts I & II," *IEEE Trans. Control Network Syst.*, vol. 1, no. 1, pp. 15–27, Mar. 2014.

[35] L. Gan and S. Low, "Convex Relaxations and Linear Approximation for Optimal Power Flow in Multiphase Radial Networks," in *18th Power Syst. Comput. Conf. (PSCC)*, Aug. 2014.

[36] M. Baran and F. Wu, "Optimal Capacitor Placement on Radial Distribution Systems," *IEEE Trans. Power Del.*, vol. 4, no. 1, pp. 725–734, Jan. 1989.

[37] Z. Li, Q. Guo, H. Sun, and J. Wang, "Sufficient Conditions for Exact Relaxation of Complementarity Constraints for Storage-Concerned Economic Dispatch," *IEEE Trans. Power Syst.*, vol. 31, no. 2, pp. 1653–1654, Mar. 2016.

[38] Z. Li , Q. Guo, H. Sun, and J. Wang, "Further Discussions on Sufficient Conditions for Exact Relaxation of Complementarity Constraints for Storage-Concerned Economic Dispatch," June 2015, arXiv:1505.02493.

[39] A. Giacomoni and B. Wollenberg, "Linear Programming Optimal Power Flow Utilizing a Trust Region Method," in *North Amer. Power Symp.*, Sept. 2010.

[40] J. Felder and I. Hiskens, "Optimal Power Flow with Storage," in *18th Power Syst. Comput. Conf. (PSCC)*, Aug. 2014.

[41] D. Molzahn, C. Josz, I. Hiskens, and P. Panciatici, "Solution of Optimal Power Flow Problems using Moment Relaxations Augmented with Objective Function Penalization," *IEEE 54th Ann. Conf. Decis. Control (CDC)*, Dec. 2015.

[42] Siemens PTI, "Volume II: Program Application Guide," *Power System Simulation for Engineering (PSS/E)*, vol. 31.0, Dec. 2007.

[43] R. Zimmerman, C. Murillo-Sánchez, and R. Thomas, "MATPOWER: Steady-State Operations, Planning, and Analysis Tools for Power Systems Research and Education," *IEEE Trans. Power Syst.*, no. 99, pp. 1–8, 2011.

[44] W. Bukhsh, A. Grothey, K. McKinnon, and P. Trodden, "Local Solutions of Optimal Power Flow Problem," *IEEE Trans. Power Syst.*, vol. 28, no. 4, pp. 4780–4788, Nov. 2013, Test Case Archive: http://www.maths.ed.ac.uk/optenergy/LocalOpt/.

[45] S. Fliscounakis, P. Panciatici, F. Capitanescu, and L. Wehenkel, "Contingency Ranking with Respect to Overloads in Very Large Power Systems Taking into Account Uncertainty, Preventive and Corrective Actions," *IEEE Trans. Power Syst.*, vol. 28, no. 4, pp. 4909–4917, Nov. 2013.

[46] E. Camacho and C. Bordons, *Model Predictive Control*, 2nd ed. New York: Springer Verlag, 2004.

[47] N. Janssens and A. Kamagate, "Loop Flows in a Ring AC Power System," in *14th Power Syst. Comput. Conf. (PSCC)*, June 2002.

[48] D. Bienstock and G. M. noz, "On Linear Relaxations of OPF Problems," *arXiv:1411.1120*, Nov. 2014.

[49] C. Coffrin and P. V. Hentenryck, "A Linear-Programming Approximation of AC Power Flows," *INFORMS J. Comput.*, vol. 26, no. 4, pp. 718–734, May 2014.

[50] F. Bouffard and F. Galiana, "Stochastic Security for Operations Planning with Significant Wind Power Generation," *IEEE Trans. Power Syst.*, vol. 23, no. 2, pp. 306–316, May 2008.

[51] A. Papavasiliou, S. Oren, and R. ONeill, "Reserve Requirements for Wind Power Integration: A Scenario-Based Stochastic Programming Framework," *IEEE Trans. Power Syst.*, vol. 26, no. 4, pp. 2197–2206, Nov. 2011.

[52] J. Morales, A. Conejo, and J. Perez-Ruiz, "Economic Valuation of Reserves in Power Systems with High Penetration of Wind Power," *IEEE Trans. Power Syst.*, vol. 24, no. 2, pp. 900–910, May 2009.

[53] L. Roald, F. Oldewurtel, T. Krause, and G. Andersson, "Analytical Reformulation of Security Constrained Optimal Power Flow with Probabilistic Constraints," in *IEEE PowerTech Conference*, June 2013.

[54] D. Bienstock and M. Chertkov and S. Harnett, "Chance-Constrained Optimal Power Flow: Risk-Aware Network Control under Uncertainty," *SIAM Review*, vol. 56, no. 3, pp. 461–495, Jan. 2014.

[55] M. Campi, S. Garatti, and F. Ramponi, "Non-Convex Scenario Optimization with Application to System Identification," in *54th IEEE Conf. Decis. Control*, Dec. 2015.

[56] M. Vrakopoulou, M. Katsampani, K. Margellos, J. Lygeros, and G. Andersson, "Probabilistic Security-Constrained AC Optimal Power Flow," in *IEEE PowerTech Conference*, June 2013.

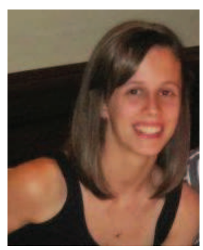

Jennifer Marley received the B.S. degree in electrical engineering with a concentration in renewable electric energy systems from North Carolina State University in 2012. She is currently pursuing a Ph.D. in Electrical Engineering: Systems at the University of Michigan. Her research interests include power system optimization and the integration of storage devices and renewable generation.

Daniel K. Molzahn (S'09-M'13) is a Computational Engineer at Argonne National Laboratory. He was a Dow Postdoctoral Fellow in Sustainability at the University of Michigan, Ann Arbor. He received the B.S., M.S., and Ph.D. degrees in electrical engineering and the Masters of Public Affairs degree from the University of Wisconsin–Madison, where he was a National Science Foundation Graduate Research Fellow. His research focuses on optimization and control of electric power systems.

Ian A. Hiskens (F'06) is the Vennema Professor of Engineering in the Department of Electrical Engineering and Computer Science, University of Michigan, Ann Arbor. He has held prior appointments in the Queensland electricity supply industry, and various universities in Australia and the United States. His research interests lie at the intersection of power system analysis and systems theory, with recent activity focused largely on integration of renewable generation and controllable loads. Dr. Hiskens is actively involved in various IEEE societies, and was VP-Finance of the IEEE Systems Council. He is a Fellow of IEEE, a Fellow of Engineers Australia and a Chartered Professional Engineer in Australia.